NSRRC - J0 4489 (2014)

Microporous and Mesoporous Materials 190 (2014) 67–73

Contents lists available at ScienceDirect

Microporous and Mesoporous Materials

journal homepage: www.elsevier.com/locate/micromeso

"pH-jump" synthesis of 2D-rectangular *c2mm* mesoporous silica materials with helical morphology and extensive void defects

Nien-Chu Lai, Chi-Jui Lin, Wei-Chia Huang, Chia-Min Yang *

Department of Chemistry, National Tsing Hua University, Hsinchu 30013, Taiwan

ARTICLE INFO

Article history:
Received 25 October 2013
Received in revised form 10 January 2014
Accepted 14 January 2014
Available online 27 January 2014

Keywords:
Mesoporous silica
c2mm symmetry
pH-jump synthesis
Void defects
In-situ small-angle X-ray scattering

ABSTRACT

Mesoporous MMT-1 silica nanoparticles with *c2mm* symmetry and helical morphology were synthesized by a "pH-jump" method using sodium silicate as silica source and ethyl acetate (and other acetate esters) as a pH modifier. In the alkaline synthesis mixture containing both cationic and nonionic surfactants at low concentration, acetate esters hydrolyzed rapidly and caused drastic drop in solution pH to initiate the cooperative assembly of silicate/surfactant mesophase and the condensation of silicate species. When ethyl acetate (EA) was used, nanoparticles with ordered *c2mm* mesostructure and helical morphology could be formed with an EA-to-silicate ratio (x) of 4.0 ~ 9.0. As x was increased from 4.0 to 9.0, the structural order was decreased yet the degree of silica condensation was enhanced. As a result, the materials exhibited much better hydrothermal stability than those synthesized from tetraalkoxysilanes (such as tetraethoxysilane). Moreover, the increase in x caused changes in particle morphology to long-pitch helical rods with increased length and increased extent of void defects that were irregular in shape and size. The differences in structural and textural properties of the MMT-1 materials should be associated with the pH drop rate and profile during the synthesis with varied x. *In-situ* small-angle X-ray scattering measurements were performed and analyzed to elucidate the formation mechanism of the materials. The results showed that the MMT-1 materials derived from the pH-jump method are promising for catalytic and other applications.

© 2014 Elsevier Inc. All rights reserved.

1. Introduction

The discoveries of helical mesoporous materials [1–9] and silica mesophases [7–12] corresponding to the intermediate phases between two-dimensional (2D)-hexagonal and lamellar phases in surfactant-water systems [13–15] are among the most fascinating and stimulating advances in the fields of porous materials [16–19] and materials chemistry in recent years. The studies on the formation of these unique materials not only give new insights into the thermodynamics and kinetics of the cooperative self-assembly of organic and inorganic species into ordered hybrids, but also bring in new opportunities in template synthesis of novel nanomaterials (e.g. helical nanowires and mesoporous materials with rarely observed mesostructures) [2,8,20] and in exploring new chemistry and phenomena (e.g. curvature-dependent chemistry in the confined space [21,22] and magnetic properties of helical metal nanowires [23,24]).

Recently, we discovered a new type of mesoporous silicas [7–9] simultaneously having helical channels and 2D-rectangular *c2mm* mesostructure that is correlated to the ribbon intermediate phases consisting of non-circular micellar rods arranged on a 2D-rectangular lattice [13–15]. The material, designated as MMT-1, can be therefore regarded as deformed structure of 2D-hexagonal mesoporous silicas such as MCM-41 [25,26] and SBA-3 [27,28]. Due to the deformation of 2D mesostructure, the channels in MMT-1 are also deformed to exhibit elliptical channel section [7–9]. The MMT-1 materials are synthesized in the alkaline and dilute solutions of mixed cationic and nonionic surfactants with tetraalkoxysilanes as silica precursor. The dimension of *c2mm* lattice of MMT-1 can be modulated in a continuous fashion by simply changing the ratio of two surfactants, and the pitch of helical channels and particle shape can be controlled by adjusting the assembly kinetics of the material [7–9]. The formation of MMT-1 may involve a microphase segregation of two types of surfactants induced by the condensation of anionic silicate species that are preferentially adsorbed by the cationic surfactant [7–9].

With unique and tunable structural and morphological features, MMT-1 materials are attractive for the design and preparation of multifunctional catalysts [29–31]. However, fast mass transport is often required for heterogeneous catalysis, and mesoporous materials with short channels [32–34] or hierarchical (or

* Corresponding author. Tel.: +886 3 5731282; fax: +886 3 5165521.
E-mail address: cmyang@mx.nthu.edu.tw (C.-M. Yang).

http://dx.doi.org/10.1016/j.micromeso.2014.01.015
1387-1811/© 2014 Elsevier Inc. All rights reserved.

multimodal) pore structure [35–41] are preferred. For mesoporous silica particles with long channels, such as those in helical mesoporous silicas, a simple yet efficient way to facilitate molecular diffusion is to introduce intra-particle porosity [38–41].

Herein we report a "pH-jump" synthesis of MMT-1 materials with extensive void defects. The synthesis strategy involves the addition of a molecule, or a pH modifier, into the highly alkaline (pH > 12) synthesis mixture (containing both silicate and surfactant) that causes a drastic pH drop to initiate cooperative assembly of silicate-surfactant mesophases. The strategy was previously employed to synthesize MCM-41 silica with bimodal mesoporosity using ethyl acetate as a pH modifier I [41,42]. In this study, we successfully adopted the "pH-jump" strategy, with acetate esters as pH modifiers, to synthesize MMT-1 nanoparticles. Interestingly, we found that the highly ordered helical materials contained extensive void defects and the density of the embedded voids, as well as the lattice dimension and particle shape, could be modulated by simply tuning amount of pH modifier. We applied *in situ* small-angle X-ray scattering (SAXS) to study the formation pathways of MMT-1 with extensive void defects. Furthermore, we found that the materials prepared by the pH-jump method exhibited higher degree of silica condensation and therefore possessed much better hydrothermal stability than those synthesized using tetraalkoxysilane as silica precursor. The results of our studies indicate that the MMT-1 materials synthesized by the pH-jump method are promising for catalytic and other applications.

2. Experimental section

2.1. Materials synthesis

The synthesis of MMT-1 materials started from the preparation of a mixture of sodium silicate (SS, $Na_2Si_3O_7$, 5.64 g, Aldrich), sodium hydroxide (NaOH, 50 wt% aqueous solution, 6.46 g, Showa), cetyltrimethylammonium bromide (CTAB, 0.85 g, Acros), tetraethylene glycol dodecyl ether ($C_{12}EO_4$, 0.3 mL, Aldrich) and water (668 mL). An acetate ester was quickly added into the mixture at 35 °C, and the resulting solution was vigorously stirred for 30 s, then kept static at 35 °C for 24 h, and finally aged at 90 °C for another 24 h. The molar composition of the synthesis solution was 1.0 SS: 0.0313 $C_{12}EO_4$: 0.0938 CTAB: 4.0 NaOH: x acetate ester: 1500 H_2O, where $x = 3.5 \sim 9.0$. Esters including methyl acetate (MA, Alfa), ethyl acetate (EA, Alfa), propyl acetate (PA, Alfa) or isopropyl acetate (IPA, Alfa) were used in this study. The solid was filtered and dried in air. For the removal of surfactants, the solids were calcined at 540 °C for 6 h.

For the evaluation of hydrothermal stability, the as-made sample (0.1 g) was transferred to a screw-capped glass bottle containing water (50 mL) and was heated at 140 °C for 24 h under stirring condition at 400 rpm. The solid was then filtered and dried at 90 °C for structural analysis.

2.2. Characterization

Powder X-ray diffraction (PXRD) patterns were recorded on a Mac Science 18MPX diffractometer using Cu Kα radiation. Scanning electron microscopy (SEM) images were obtained with a field emission JEOL JSM-7000F microscope operating at 10 kV. The samples were coated with platinum before measurements. Transmission electron microscopy (TEM) images were taken from ultramicrotomed samples (thickness of 80–100 nm, supported on carbon-coated copper grids) by using a JEOL JEM-2010 microscope operated at 200 kV. Nitrogen physisorption isotherms were measured at 77 K using a Quantachrome Autosorb-1MP instrument. The isotherms were analyzed by nonlocal density functional theory (NLDFT) (by applying a N_2 (77 K) kernel based on cylindrical pore geometry) to evaluate the pore size and surface area of the samples. The total pore volume was evaluated at a relative pressure (p/p_0) of 0.9. Solid-state ^{29}Si MAS NMR spectra were measured on a Bruker DSX400WB spectrometer using a 7-mm probe. *In-situ* SAXS measurements were performed at the beamline 23A1 of the National Synchrotron Radiation Research Center (NSRRC), Taiwan, using X-ray with a photon energy of 10.0 keV. The synthesis mixture obtained after the addition of EA followed by 30-s stirring was poured into a thermostated (30 °C) Kapton-sealed thin container, through which the X-ray beam passed. One-dimensional SAXS profiles were circularly averaged from 2D images obtained using a multiwire area detector (gas-type). The sample-to-detector distance was 1830 mm. The scattering wavevector q, $4\pi \sin(\theta)/\lambda$, defined by the scattering angle 2θ and wavelength λ, was calibrated with silver behenate, and the scattering intensity $I(q)$ was calibrated to the absolute intensity scale with a polyethylene sample.

3. Results and discussion

We first investigated the influences of the type of pH modifier on the structural properties of the resulting materials. Fig. 1 shows the PXRD patterns of the samples synthesized with MA, EA, PA and IPA with an ester-to-silicate ratio (x) = 4.0. All the samples except the one synthesized with IPA exhibited well-resolved reflections in the 2θ range of 1–5° that can be perfectly indexed with 2D-rectangular *c2mm* lattices (cf. inset in Fig. 1). The derived lattice parameters b for the MMT-1 samples were almost identical (~4.4 nm), whereas the parameter a increased from 10.2 nm for the sample synthesized with MA to 10.9 nm for that with PA. This indicated an increase in the degree of structural deformation, as compared to a 2D-hexagonal lattice with $a/b = \sqrt{3}$, when changing the pH modifier from MA (a/b = 2.32) to PA (a/b = 2.55). The distinct structural properties of the series of samples should be associated with the hydrolysis rate of the acetate esters and the type of alcohol thus generated. The hydrolysis rate of acetate esters in the alkaline synthesis mixture determines the pH profile (or the change in pH with reaction time) which in turn affects the rate and extent of silicate condensation and cooperative silicate-surfactant assembly.

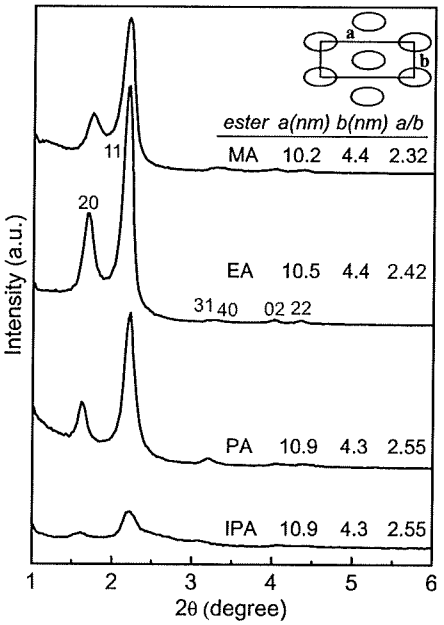

Fig. 1. PXRD patterns for the as-synthesized materials with varied acetate esters.

The rate constants of alkaline hydrolysis of MA, EA, PA and IPA, reported by Mill et al., are 0.182, 0.110, 0.087, and 0.030 $M^{-1} s^{-1}$, respectively [43]. It seems that an ester with a hydrolysis rate faster than that of IPA is required for the successful formation of MMT-1 materials. On the other hand, depending on molecular polarity, the alcohol generated by ester hydrolysis could either dissolve in the aqueous synthesis mixture or penetrate into the palisade layer of surfactant micelles to affect the structure of hybrid mesophases [44]. Our previous investigations suggest that a microphase segregation of CTAB and $C_{12}EO_4$ takes place during the formation of the *c2mm* mesophase owing to the preferential adsorption of anionic silicate species onto cetyltrimethylammonium (CTA) cations, resulting in deformed silicate-encased micellar rods with the $C_{12}EO_4$-enriched flattened parts and the CTA-enriched highly curved parts [7–9]. In this study, the observed increase of the lattice parameter *a* with increasing the carbon number of acetate ester should be mainly associated with the polarity-dependent behavior of alcohols generated from the esters: the lower the polarity of the alcohol is, the greater the tendency for the alcohol to penetrate and preferentially stay at the $C_{12}EO_4$-enriched flattened parts of micellar rods would be.

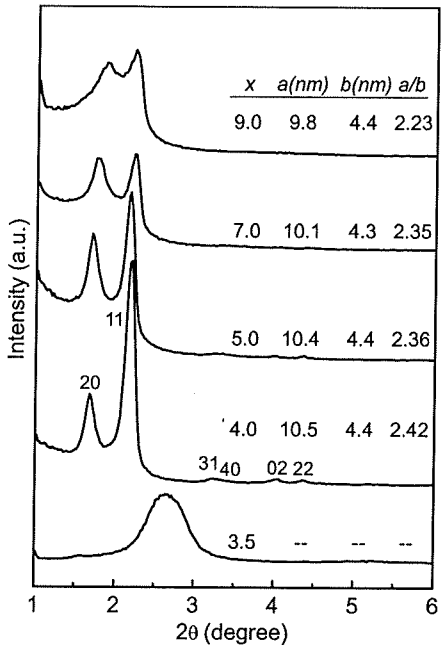

Fig. 2. PXRD patterns for the as-synthesized materials with varied amount of EA.

We next examined the synthesis with varied amount of ester pH modifier since that would influence the profile of pH drop and the final pH of the synthesis mixture. We chose EA for the study because the sample synthesized with EA exhibited the best structural order. As evidenced by PXRD shown in Fig. 2, the amount of EA is crucial for forming ordered mesostructure of MMT-1 and the ester-to-silicate ratio (x) below 4.0 resulted in materials with lamellar or disordered structure. For the synthesis with $x = 3.5$, the final solution pH was 10.1 and the yield of the sample was only about 35% (based on silica weight). In comparison, the final solution pH was 9.3 and the yield was ~75% for the synthesis with $x = 4.0$. The low yields of disordered samples synthesized with $x < 4.0$ could be understood by considering the pH-dependent dissolution/condensation equilibrium of silicate in alkaline solutions [45]. As x was increased to 5.0, 7.0 and 9.0, the final solution pH was decreased (to 7.4, 7.1 and 7.0, respectively) and the yield became higher (~95% for the synthesis with $x = 9.0$). However, the increase of x also led to a drop in the intensities of X-ray reflection peaks (especially 11 reflection), decreased intensity ratio of 11 and 20 reflections, and slight decreased lattice parameter *a*. Although the reflections became more intense for the calcined samples (cf. Fig. S1 in the Supplementary Materials), the trends remained the same.

The observed trends in PXRD might be associated with possible changes in textural and/or morphological properties of the materials [8,9]. To examine the speculation, electron microscopies and nitrogen physisorption were further applied for the characterization of the samples. Fig. 3 shows the SEM and TEM images of the three samples synthesized with varied amount of EA (cf. Fig. S2 in the Supplementary Materials for low-magnification SEM and TEM images). Obviously, the amount of pH modifier affected simultaneously both the morphology and porous texture of the resulting MMT-1. The sample synthesized with $x = 4.0$ contained spherical particles with circular stripes on the surface, similar to those in the MMT-1 with short-pitch (just a few lattice constants) helical channels [7,8]. As x was increased to 5.0, the particle shape

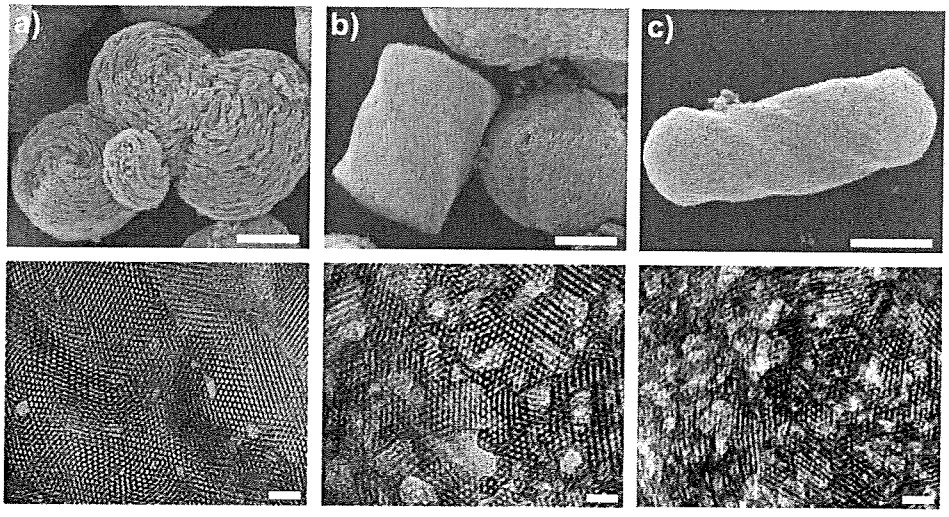

Fig. 3. SEM images (top) of the as-synthesized MMT-1 and TEM images (down) of the ultramicrotomed calcined MMT-1 synthesized with $x = 4.0$ (a), 5.0 (b), and 9.0 (c). Scale bars indicate 500 nm in SEM images or 25 nm in TEM images.

was transformed to helical rods with diameters of ~750 nm and helical pitches of ~500 nm. The corresponding pitch-to-diameter (P/D) ratio is about 0.70, which is smaller than the values for long-pitch MMT-1 twisted/spiral rods ($P/D \sim 3.5$) [8] and most reported MCM-41-like helical materials ($P/D \sim 6.0$) [3,4,6]. The morphology remained except an increase in the aspect ratio for the rods observed in the sample with synthesized $x = 9.0$. Furthermore, the TEM images of the ultramicrotomed samples revealed the presence of void defects in the interior of these samples. While only a few small and isolated voids were observed in the sample synthesized with $x = 4.0$, extensive voids with irregular shape and sizes ranging from 10 to 120 nm existed in those synthesized with $x = 5.0$ and 9.0. In consistence with TEM observation, nitrogen physisorption analysis confirmed the presence of intra-particle porosities. As shown in Fig. 4, all the isotherms are type IV curves exhibiting steps over the relative pressure (p/p_0) at 0.25–0.35 and hysteresis loops at $p/p_0 = 0.5$–1.0. The steps may be attributed to the channel-type mesopores, and the pore sizes for the three samples derived by the NLDFT method are 3.7 nm. On the other hand, the isolated voids in the sample synthesized with $x = 4.0$ behaved like ink-bottle-type pores and gave rise to the H2-type hysteresis, and the extensive voids in the samples with $x = 5.0$ and 9.0 lead to the H3-type hysteresis. The bimodal mesoporosity in the samples with $x = 5.0$ and 9.0 was further confirmed by their pore size distributions showing a sharp peak at 3.7 nm and a wide distribution over 6–30 nm (inset of Fig. 4).

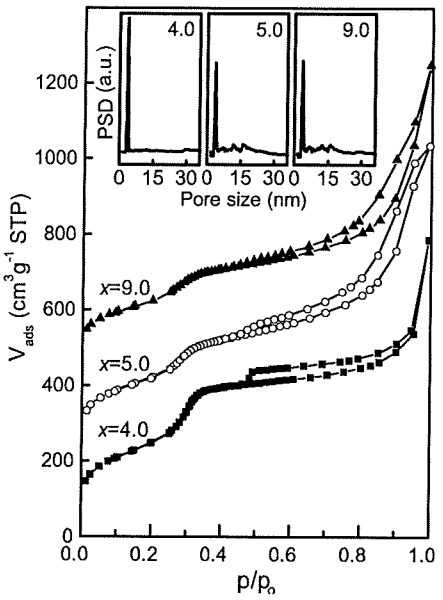

Fig. 4. Nitrogen physisorption isotherms of MMT-1 materials synthesized with varied amount of EA. The isotherms are shifted by 0, 200 and 450 cm^3 g^{-1} STP, respectively.

The structural evolution during the pH-jump synthesis of MMT-1 materials with $x = 4.0$, 5.0 and 9.0 was also studied by *in situ* SAXS, and the patterns recorded at a reaction time (t) up to 20 min are shown in Fig. 5. In all three cases, a Bragg peak appeared at around $q = 0.1421$ Å^{-1} ($d = 4.5$ nm) after a period of time (defined as the induction time t_{ind}) from the addition of EA at $t = 0$ min. The peak remained at the same position and became more intense within the following several minutes (defined as Δt_1) before starting to split into two. The two peaks further moved away from each other and got stronger during the subsequent period of time (defined as Δt_2), after which they stopped shifting and growing accompanied with the appearance of additional weak peaks at high-q range. The patterns recorded during Δt_2 and at $t = 20$ min could be indexed assuming a 2D-rectangular *c2mm* lattice, and the lattice parameters a and b were derived from the 20 and 11 peaks. A rate constant k_{def} for the structural deformation during Δt_2 could be then calculated from the plot of a/b ratio versus time (cf. Fig. S3 in the Supplementary Materials) by assuming a pseudo-first-order kinetics [8]. Moreover, in order to estimate the rate of materials growth (or called crystallization), the change of the intensity of the 11 peak was further analyzed by applying the Avrami–Erofe'ev expression [46–48], a widely applied expression to model the formation of various microporous and mesoporous materials [8,46–48]:

$$\alpha = \frac{I_{hkl}(t)}{I_{hkl}(\max)} = 1 - exp[-(k_c(t - t_{ind}))^n] \quad (1)$$

where α is the extent of reaction ($0 \leqslant \alpha \leqslant 1$), k_c is the rate constant of the crystallization, and n is the Avrami exponent correlated to the dimensionality of nuclei growth, and the value of α was derived

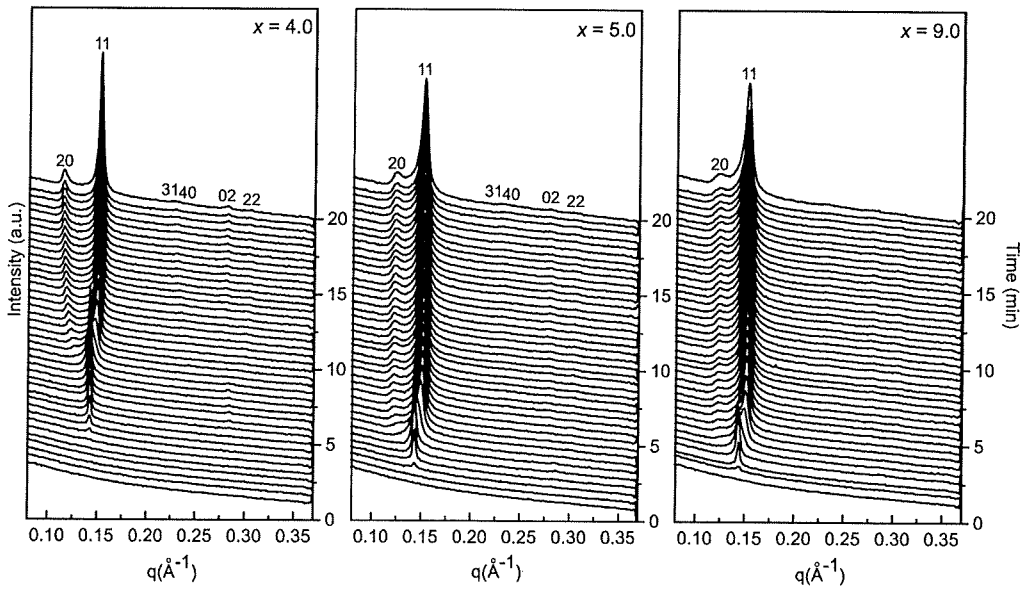

Fig. 5. *In-situ* SAXS measurements of the synthesis of MMT-1 with varied amount of EA.

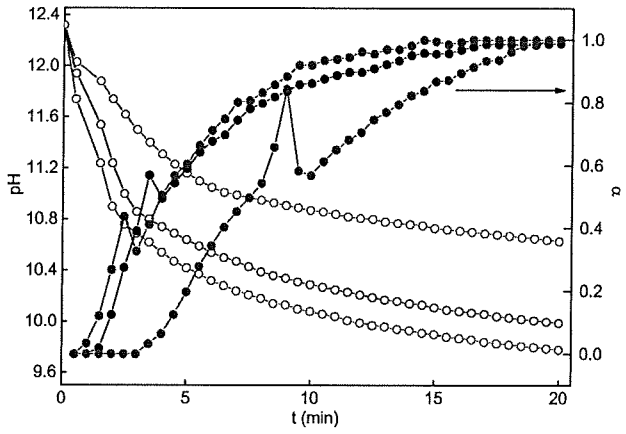

Fig. 6. Avrami plots (closed circle) and recorded solution pH (open circle) for the synthesis MMT-1 materials with $x = 4.0$ (red), 5.0 (blue) and 9.0 (green). (For interpretation of the references to color in this figure legend, the reader is referred to the web version of this article.)

from the peak areas at time t ($I_{hkl}(t)$) and the maximum area of this peak ($I_{hkl}(\max)$) [46–48]. Fig. 6 shows the resulting Avrami plots. A sudden drop in α after the splitting of the peak at the end of Δt_1 might be associated to the change in the X-ray scattering power of the evolving organic–inorganic hybrids, and that part of data was ignored for kinetic analysis. All the parameters derived from *in situ* SAXS are summarized in Table 1. Obviously, an increase in the amount of EA (especially when increasing x from 4.0 to 5.0) resulted in faster drop of the solution pH (cf. Fig. 6), which speeded up not only the nucleation and growth of ordered organic–inorganic hybrids (with shorter t_{ind}, Δt_1 and Δt_2 and larger k_{def} and k_c) but also the silica condensation rate to result in *c2mm* mesostructure with lower degree of structural deformation (i.e. smaller a/b ratio). It is noteworthy that the onset of materials growth coincided with a pH drop to ~11.5 and that the structural deformation began at pH = 10.8–11.0. It is known that the solution pH greatly affects the distribution of silicate species with varied size and charge that may in turn influence the condensation processes of these species and the interactions with surfactant molecules. Hence, there seemed to exist an optimum distribution of various silicate species in the synthesis solution to initiate simultaneously silica condensation and the cooperative assembly with CTAB and $C_{12}EO_4$ and subsequently induce microphase segregation of the two surfactants.

The *in situ* SAXS measurements, together with other characterization results, provide some insight to the formation of the MMT-1 materials simultaneously having regular morphology yet void defects. The formation of void defects with irregular shape and sizes is not likely to take place prior to the development of helical morphology, involving the packing and growth of bent and coiled silicate-encased micellar rods, that is mainly driven by the reduction in surface free energy (ΔG_S) [8]. For the synthesis of helical MMT-1 nanostructures without void defects using tetraethoxysilane (TEOS) as silica precursor, we found that the morphology development and structural deformation started almost simultaneously at an extent of material growth (α) of ~0.4–0.5 [8]. Distinctly, in the pH-jump synthesis with varied amount of EA, similar values of α were reached within the time period Δt_1. Besides, the sudden drop of α at the end of Δt_1 may be most likely to be correlated to the initiation of void formation that may decrease the extent of structural order leading to an intensity drop of the SAXS peak. Based on the discussion, we believe that the helical morphology of the MMT-1 materials synthesized by the pH-jump method was mainly developed during Δt_1, after which structural deformation and void formation took place roughly at the same time. Moreover, the slow change of solution pH in the synthesis with $x = 4.0$ may allow the formation of thermodynamically more stable morphology, which is the short-pitch helical particle with lower ΔG_S. On the contrary, faster pH drop with $x = 5.0$ and 9.0 resulted in long-pitch particles with higher ΔG_S. As for the formation of void defects, we speculate that it should be linked to the inhomogeneity of solution pH during materials growth. After helical morphology was almost developed, the solution pH kept on decreasing and the rate of silicate condensation continued to increase. However, the condensation reaction released hydroxyl ions (OH^-), and the ions generated at the inner part of the growing particles may not be easily neutralized in comparison to those at the periphery of particles. The inconsistency would lead to the inhomogeneity in the degree of silica condensation across the particles and cause the formation of defects or voids to release strain possibly built up in the particles. The larger the amount of EA added, the greater the inhomogeneity would be and subsequently the more void defects were formed. The proposed formation mechanism could satisfactorily explain our observations, and more studies may be needed to further verify it.

In addition to the unique morphological and textural features, the MMT-1 materials synthesized by the pH-jump method also exhibited higher degree of silica condensation as compared to those synthesized with TEOS as silica source [7,8]. Fig. 7 shows the ^{29}Si MAS NMR spectra of the three samples synthesized with varied amount of EA and the sample (labeled as E-MMT-1) synthesized with TEOS under similar conditions (with the same concentrations of surfactants and silica source and aging

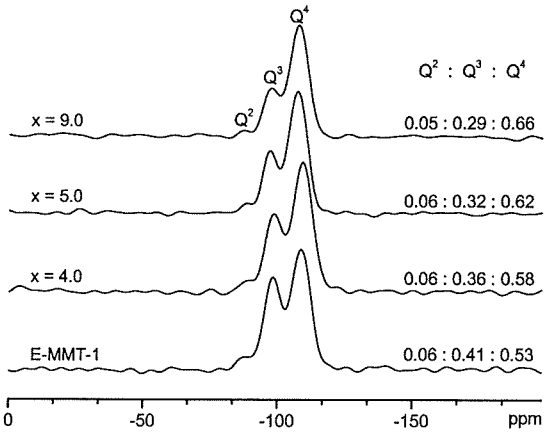

Fig. 7. ^{29}Si MAS NMR spectra of the MMT-1 samples synthesized by the pH-jump method with varied amount of EA and the sample (E-MMT-1) synthesized using TEOS as silica source.

Table 1
Parameters derived from *in situ* SAXS for the pH-jump synthesis with varied amount of EA.

x	t_{ind} (min)	Δt_1 (min)	Δt_2 (min)	a (nm)	b (nm)	a/b	k_{def} (10^{-3} s^{-1})	k_c (10^{-3} s^{-1})
4.0	4	5.5	6	10.8	4.5	2.41	1.1	2.8
5.0	2	2.5	3	10.4	4.5	2.31	3.4	6.7
9.0	1.5	2	2	10.3	4.5	2.29	3.7	7.3

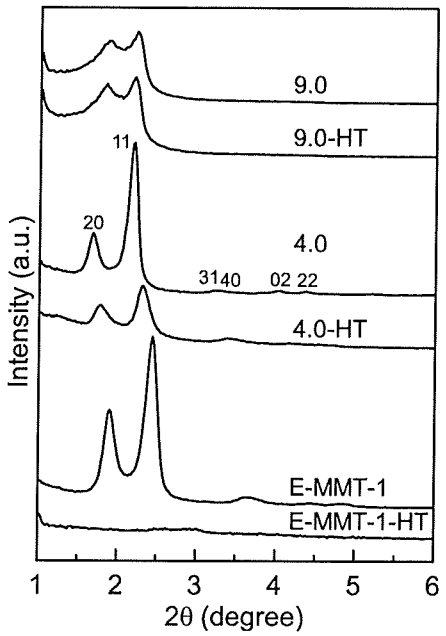

Fig. 8. PXRD patterns of MMT-1 samples synthesized with different silica source under hydrothermal condition.

temperature, solution pH ~ 10.2). These spectra were deconvoluted to obtain the relative intensities of the lines attributed to the various Q^n groups ($Si(OSi)_n(OH)_{4-n}$, $n = 2,3,4$), and the intensity ratio are also shown in the figure. As compared to the spectrum of E-MMT-1, the spectra of the samples derived from the pH-jump synthesis showed more intense Q^4 lines and weaker Q^3 lines and the intensity of Q^4 line became higher with increasing x. The difference in the degree of silica condensation can be comprehended by knowing that the silica condensation rate is maximized near neutral pH [45] and that, as aforementioned, the synthesis with $x = 4.0$, 5.0 and 9.0 showed final solution pH of 9.3, 7.4 and 7.0, respectively. With the results, the hydrothermal stability of the as-synthesized samples was examined by heating them at 140 °C for one day. As indicated by the PXRD patterns in Fig. 8, a complete loss of mesoscopic ordering was observed for E-MMT-1 after the hydrothermal treatment (designated as E-MMT-1-HT). On the contrary, the *c2mm* mesostructure of the samples synthesized by the pH-jump method was retained and the hydrothermally-treated sample with $x = 4.0$ (designated as 4.0-HT) only showed slight decreases in lattice parameters (~5.2% for both a and b) and structural order (leading to ~20% decrease in the reflection intensity). Notably, in spite of the presence of extensive void defects, the sample synthesized with $x = 9.0$ exhibited negligible change in its ordered mesostructure after the treatment and gave a PXRD pattern that is nearly identical to that of the as-synthesized sample. The superior hydrothermal stability was also observed for the MCM-41 sample synthesized by the pH-jump method (cf. Fig. S4 in the Supplementary Materials). The results indicate that the pH-jump synthesis can be applied to prepare MMT-1 and other mesoporous silica materials with high stability and controlled mesostructural, textural and morphological properties for catalytic and other applications.

4. Conclusions

A "pH-jump" method has been discovered to prepare MMT-1 materials simultaneously with *c2mm* mesostructure, helical morphology and extensive void defects. The method involves the usage of sodium silicate as silica source and ethyl acetate or other acetate esters as pH modifier. When ethyl acetate was used, MMT-1 nanoparticles with long-pitch rod morphology and 10–120 nm irregularly-shaped void defects would be synthesized. The MMT-1 materials had higher degree of silica condensation and therefore exhibited much better hydrothermal stability than those synthesized by using tetraethoxysilane. With extensive defect yet high hydrothermal stability, the MMT-1 materials derived from the pH-jump method are promising for catalytic and other applications.

Acknowledgement

The authors thank the National Science Council of the Republic of China for financial support under contract No. NSC98-2113-M-007-020-MY3.

Appendix A. Supplementary data

Supplementary data associated with this article can be found, in the online version, at http://dx.doi.org/10.1016/j.micromeso.2014.01.015.

References

[1] Q.S. Huo, D.Y. Zhao, J.L. Feng, K. Weston, S.K. Buratto, G.D. Stucky, S. Schacht, F. Schüth, Adv. Mater. 9 (1997) 974–978.
[2] S. Che, Z. Liu, T. Ohsuna, K. Sakamoto, O. Terasaki, T. Tatsumi, Nature 429 (2004) 281–284.
[3] B. Wang, C. Chi, W. Shan, Y.H. Zhang, N. Ren, W.L. Yang, Y. Tang, Angew. Chem. Int. Ed. 45 (2006) 2088–2090.
[4] S. Yang, L. Zhao, C. Yu, X. Zhou, J. Tang, P. Yuan, D. Chen, D. Zhao, J. Am. Chem. Soc. 128 (2006) 10460–10466.
[5] G.-L. Lin, Y.-H. Tsai, H.-P. Lin, C.-Y. Tang, C.-Y. Lin, Langmuir 23 (2007) 4115–4119.
[6] P. Yuan, L. Zhao, N. Liu, G. Wei, Y. Wang, G.J. Auchterlonie, J. Drennan, G.Q. Lu, J. Zou, C. Yu, Chem. Eur. J. 16 (2010) 1629–1637.
[7] C.M. Yang, C.Y. Lin, Y. Sakamoto, W.C. Huang, L.L. Chang, Chem. Commun. (2008) 5969–5971.
[8] W.-C. Huang, L.-L. Chang, Y. Sakamoto, C.-Y. Lin, N.-C. Lai, C.-M. Yang, RSC Adv. 1 (2011) 229–237.
[9] W.-C. Huang, N.-C. Lai, L.-L. Chang, C.-M. Yang, Microporous Mesoporous Mater. 151 (2012) 411–417.
[10] D.Y. Zhao, Q.S. Huo, J.L. Feng, J.M. Kim, Y.J. Han, G.D. Stucky, Chem. Mater. 11 (1999) 2668–2672.
[11] H.B. Qiu, Y. Sakamoto, O. Terasaki, S.N. Che, Adv. Mater. 20 (2008) 425–429.
[12] Y. Han, D. Zhang, L.L. Chng, J. Sun, L. Zhao, X. Zou, J.Y. Ying, Nat. Chem. 1 (2009) 123–127.
[13] F. Husson, H. Mustacchi, V. Luzzati, Acta Crystallogr. 13 (1960) 668–677.
[14] H. Hagslatt, O. Soderman, B. Jonsson, Liq. Cryst. 12 (1992) 667–688.
[15] S. Gustafsson, P.O. Quist, B. Halle, Liq. Cryst. 18 (1995) 545–553.
[16] G.J.D. Soler-illia, C. Sanchez, B. Lebeau, J. Patarin, Chem. Rev. 102 (2002) 4093–4138.
[17] F. Hoffmann, M. Cornelius, J. Morell, M. Fröba, Angew. Chem. Int. Ed. 45 (2006) 3216–3251.
[18] B.G. Trewyn, I.I. Slowing, S. Giri, H.-T. Chen, V.S.Y. Lin, Acc. Chem. Res. 40 (2007) 846–853.
[19] T. Kimura, K. Kuroda, Adv. Funct. Mater. 19 (2009) 511–527.
[20] C.M. Yang, H.S. Sheu, K.J. Chao, Adv. Funct. Mater. 12 (2002) 143–148.
[21] M.K. Kidder, P.F. Britt, A.L. Chaffee, A.C. Buchanan III, Chem. Commun. (2007) 52–54.
[22] R. Dabestani, M. Kidder, A.C. Buchanan III, J. Phys. Chem. C 112 (2008) 11468–11475.
[23] I. Martin, A.F. Morpurgo, Phys. Rev. B 85 (2012) 144505.
[24] S.V. Grigoriev, N.M. Potapova, S.A. Siegfried, V.A. Dyadkin, E.V. Moskvin, V. Dmitriev, D. Menzel, C.D. Dewhurst, D. Chernyshov, R.A. Sadykov, L.N. Fomicheva, A.V. Tsvyashchenko, Phys. Rev. Lett. 110 (2013) 207201.
[25] J.S. Beck, J.C. Vartuli, W.J. Roth, M.E. Leonowicz, C.T. Kresge, K.D. Schmitt, C.T.W. Chu, D.H. Olson, E.W. Sheppard, S.B. McCullen, J.B. Higgins, J.L. Schlenker, J. Am. Chem. Soc. 114 (1992) 10834–10843.
[26] C.T. Kresge, M.E. Leonowicz, W.J. Roth, J.C. Vartuli, J.S. Beck, Nature 359 (1992) 710–712.
[27] Q.S. Huo, D.I. Margolese, U. Ciesla, P.Y. Feng, T.E. Gier, P. Sieger, R. Leon, P.M. Petroff, F. Schüth, G.D. Stucky, Nature 368 (1994) 317–321.
[28] S.M. Yang, H. Yang, N. Coombs, I. Sokolov, C.T. Kresge, G.A. Ozin, Adv. Mater. 11 (1999) 52–55.
[29] C.-M. Yang, H.-A. Lin, B. Zibrowius, B. Spliethoff, F. Schüth, S.-C. Liou, M.-W. Chu, C.-H. Chen, Chem. Mater. 19 (2007) 3205–3211.

[30] H.-A. Lin, C.-H. Liu, W.-C. Huang, S.-C. Liou, M.-W. Chu, C.-H. Chen, J.-F. Lee, C.-M. Yang, Chem. Mater. 20 (2008) 6617–6622.
[31] C.-H. Liu, Y. Guan, E.J.M. Hensen, J.-F. Lee, C.-M. Yang, J. Catal. 282 (2011) 94–102.
[32] B.C. Chen, H.P. Lin, M.C. Chao, C.Y. Mou, C.Y. Tang, Adv. Mater. 16 (2004) 1657–1661.
[33] Sujandi, E.A. Prasetyanto, S.-E. Park, Appl. Catal. A: Gen. 350 (2008) 244–251.
[34] S.-Y. Chen, C.-Y. Huang, T. Yokoi, C.-Y. Tang, S.-J. Huang, J.-J. Lee, J.C.C. Chan, T. Tatsumi, S. Cheng, J. Mater. Chem. 22 (2012) 2233–2243.
[35] Z.Y. Yuan, J.L. Blin, B.L. Su, Chem. Commun. (2002) 504–505.
[36] G.L. Drisko, A. Zelcer, R.A. Caruso, G.J.d.A.A. Soler-Illia, Microporous Mesoporous Mater. 148 (2012) 137–144.
[37] D.-S. Moon, J.-K. Lee, Langmuir 28 (2012) 12341–12347.
[38] H.P. Lin, S.T. Wong, C.Y. Mou, C.Y. Tang, J. Phys. Chem. B 104 (2000) 8967–8975.
[39] J.L. Zheng, S.R. Zhai, Y. Zhang, D. Wu, Y.H. Sun, Y.X. Yang, L. Chen, F. Deng, Catal. Today 93–95 (2004) 529–534.
[40] Y.-C. Hsu, Y.-T. Hsu, H.-Y. Hsu, C.-M. Yang, Chem. Mater. 19 (2007) 1120–1126.
[41] C. Bernal, M. Mesa, M. Jaber, J.L. Guth, L. Sierra, Microporous Mesoporous Mater. 153 (2012) 217–226.
[42] H. Drossman, H. Johnson, T. Mill, Chemosphere 17 (1988) 1509–1530.
[43] A. Chang, N.-C. Lai, C.-M. Yang, RSC Adv. 2 (2012) 12088–12090.
[44] C.J. Brinker, G.W. Scherer, Sol-Gel Sci. 1990, pp. 99–228 (Chapter 3).
[45] M. Avrami, J. Chem. Phys. 7 (1939) 1103–1112.
[46] M. Avrami, J. Chem. Phys. 8 (1940) 212–224.
[47] M. Avrami, J. Chem. Phys. 9 (1941) 177–184.
[48] B.V. Erofe'ev, C.R. Dokl, Acad. Sci. URSS 52 (1946) 511–517.